3D-Printable Dielectric Transmitarray With Enhanced Bandwidth at Millimeter-Waves

IEEE Access
Multidisciplinary | Rapid Review | Open Access Journal

Received June 22, 2018, accepted August 3, 2018, date of publication August 13, 2018, date of current version September 7, 2018.

Digital Object Identifier 10.1109/ACCESS.2018.2865353

3D-Printable Dielectric Transmitarray With Enhanced Bandwidth at Millimeter-Waves

ANDREA MASSACCESI[1], (Student Member, IEEE), PAOLA PIRINOLI[1], (Member, IEEE), VALENTINA BERTANA[2], GIORGIO SCORDO[2], SIMONE LUIGI MARASSO[3], MATTEO COCUZZA[3], AND GIANLUCA DASSANO[1]

[1]Department of Electronics and Telecommunications, Politecnico di Torino, 10129 Turin, Italy
[2]Chilab-Materials and Microsystems Laboratory, Department of Applied Sciences and Technology, Politecnico di Torino, 10129 Turin, Italy
[3]IMEM-CNR, 43124 Parma, Italy

Corresponding author: Andrea Massaccesi (andrea.massaccesi@polito.it)

This work was supported by the General Directorate for Cultural and Economic Promotion and Innovation of the Ministry of Foreign Affairs and International Cooperation of the Italian Republic.

ABSTRACT In this paper, a three-layer dielectric structure is presented as innovative unit-cell element for transmitarray (TA) antennas with enhanced bandwidth. It consists of a central layer, with a varying size square hole, used to compensate the phase of the incident field and located between two other identical layers with linearly tapered square holes, acting as matching circuits. The effectiveness of this unit-cell is demonstrated by the numerical and the experimental results here presented. As a first step, three different TAs with increasing size are designed and simulated: their 1-dB gain bandwidth, centered at 30 GHz, varies from the 30.9% of the smallest configuration, having size of $10\lambda_0 \times 10\lambda_0$, to the 17.5% of the $20\lambda_0 \times 20\lambda_0$ TA. A slightly modified unit-cell is then designed, with the aim of realizing a prototype with an additive manufacturing (AM) technique. A 3D-printed dielectric TA with a size of $15.6\lambda_0 \times 15.6\lambda_0$ has been manufactured and experimentally characterized. The measured prototype shows excellent performances, achieving a 1-dB gain bandwidth of 21.5%: these results prove the enhanced features of the introduced unit-cell and demonstrate the TA feasibility with AM techniques.

INDEX TERMS Wideband antenna, transmitarray antenna, planar lens, discrete lens, tapered matching, 3D-printed antenna, 3D-printing.

I. INTRODUCTION

Transmitarrays are becoming an emerging and attractive solution for realizing high-gain, low profile and beam steering antennas. A transmitarray (TA) antenna consists of an illuminating feed source and a quasi-periodic transmitting planar surface that transforms the incoming wave into a desired outgoing one. Thanks to its characteristics, which allow to exploit the advantages of lenses and phased arrays, TA is a valid candidate to be a low-cost antenna for satellite communication operating in X, Ku, K and Ka-bands. Compared to a reflectarray, it does not suffer for feed blockage and it has a better tolerance to surface errors [1]–[16]. TAs can be realized adopting the same techniques used for reflectarrays: they can be made-up of several layers (at least three) of printed elements, whose size is varied to transform the incident spherical wave in a planar one, or they can consist in just two parallel arrays (a receiving and a transmitting one) of microstrip resonant patches that are coupled through apertures and stripline delay lines [2], or vias [3].

As for reflectarrays, one of the main drawbacks of transmitarrays is their limited bandwidth, due to the intrinsic narrow band of the single radiating element and to the frequency dependence of the spatial phase delay of the paths from the feed to each TA element. In order to overcome this problem, several solutions have been proposed. A four-layer transmitarray using dual-resonant double square rings as unit-cell element was presented in [4]: it provides a 7.5% 1-dB gain bandwidth when used to design a square TA with size of $12.6\lambda_0 \times 12.6\lambda_0$. In [5], a reduced size TA composed by three layers of spiral dipoles exhibits a 1-dB gain bandwidth of 9%. Similar results are achieved in [6], where a $5.4\lambda_0 \times 5.4\lambda_0$ transmitarray using split diagonal cross element has a 9.6% 1-dB gain bandwidth. Novel methods to improve the bandwidth controlling the transmission phase range and

optimizing the phase distribution on the array aperture are described in [7]: two quad-layer circular transmitarrays with moderate size were designed to reach 9.8% and 11.7% 1-dB gain bandwidths. A linearly polarized slot-based transmitarray using three thin metal layers interposed by air gaps provides a bandwidth of 15.5% [8]. The TA proposed in [9] consists of a planar circular array printed on a three-metal layer circuit board, an ad-hoc focal source and a radome layer: this configuration has an aperture diameter of 20.5λ and it is characterized by a 15.4% 1-dB gain bandwidth. In [10], a triple-layer circular TA combining cross slot elements and double square loops achieves 16.8% of 1-dB gain bandwidth.

Another possible technological solution for the realization of a transmitarray is the adoption of perforated dielectric layer(s) [11]–[16]. In this solution, which can be alternatively named flat lens, the phase of the incident field can be controlled changing the size of the holes, and therefore the local effective dielectric constant of the substrate. The results related to the design of lenses and reflectarrays consisting in a single dielectric layer of elements made with four equally-spaced circular holes are reported in [12] and [13]. The performances of multilayer perforated dielectric lenses using a four-hole unit-cell are presented in [14]. A similar technique is exploited to design a 3-D printed dielectric lens using variable-height elements and square anti-reflection structures [15]. An alternative approach to design a perforated dielectric transmitarray is described in [16], where the adopted unit-cell is made-up of a central dielectric layer with a varying size square hole used to control the phase of the transmission coefficient S_{21}, and two external matching layers behaving as quarter-wave impedance transformers and aimed to increase S_{21} magnitude. Despite of the improvements achieved for the transmission coefficient, the introduction of the matching layers, which are intrinsically narrow band, causes a considerable reduction of the TA bandwidth.

In this paper, a novel perforated dielectric transmitarray configuration is introduced. The proposed unit-cell consists of a triple-layer perforated dielectric element: similarly to [16], in the middle layer there is a square hole, whose variable size W is used to compensate the phase of the incident field, while the external layers present a truncated pyramid hole with the smaller basis having size W and simulating a tapered matching circuit. The addition of these tapered structures allows to improve the performances of the TA for what concerns its bandwidth.

The unit-cell is described in the Section II-A, while its use in the design of center-fed TAs of different size and working in Ka-band, is presented in Section II-B. The results of their numerical analysis demonstrate the effectiveness of the proposed solution that provides significant performance improvements compared with other configurations available in literature. In view of them, a slightly modified and 3D-printable version of the unit-cell is introduced in III-B. A $15.6\lambda_0 \times 15.6\lambda_0$ TA working in Ka-band at 30 GHz has been manufactured and experimentally validated. The obtained results are discussed in III-C.

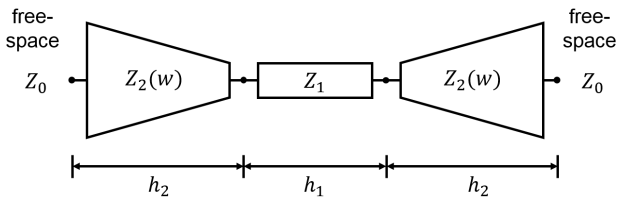

FIGURE 1. Equivalent transmission line model of the proposed three-layers unit-cell shown in Figure 2.

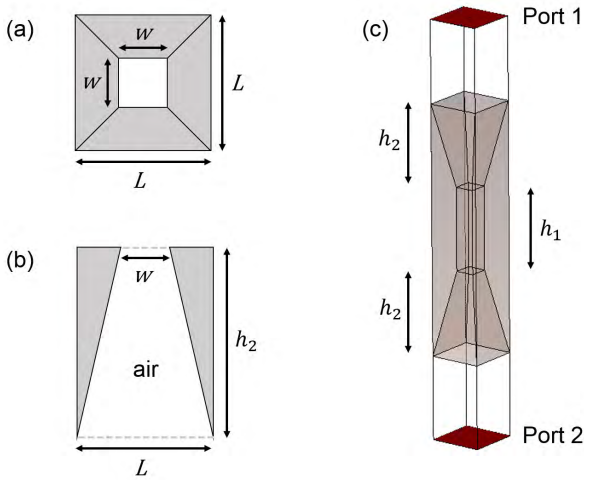

FIGURE 2. Transmitarray unit-cell: (a) Top view; (b) Side view of one of the two layers with truncated pyramid hole; (c) 3D view of the cell simulated in CST MW Studio.

II. WIDEBAND TRANSMITARRAY

A. DIELECTRIC UNIT-CELL

To avoid the band limitations of the dielectric unit-cell introduced in [11]–[16], in this work an alternative solution is investigated. From transmission line theory, it is well-known that the impedance transformer bandwidth limitation can be overcome using a tapered transmission line, i.e. a transmission line whose characteristic impedance varies continuously according to a predefined profile, that is in most cases linear or exponential. This concept is applied here to design a three-layer TA unit-cell. Its equivalent transmission line model is sketched in Fig. 1: the characteristic impedance Z_1 of the central and uniform transmission line is matched to the free-space impedance Z_0 through two linearly tapered transmission lines whose characteristic impedance Z_2 varies with the section w of the transmission line itself. A good matching can be realized choosing the length h_2 of the tapered lines at least equal to $\lambda_g/2$ where λ_g is the effective wavelength in the tapered section.

The corresponding perforated dielectric unit-cell is shown in Fig. 2. The central section presents a square hole with a constant size W along its length h_1 and it is equivalent to the central transmission line in the schematic of Fig. 1. The phase of the incident field can be compensated varying W. In the two external layers, the hole has the shape of a truncated pyramid: the larger basis has a fixed size L, the smaller basis

has the same size W of the central layer hole, while the truncated pyramid height is h_2. In this way, it is possible to realize linearly tapered transmission lines as those in the equivalent model in Fig. 1.

In order to determine the optimal values of the unit-cell geometrical parameters, its analysis has been carried out varying L, h_1 and h_2. The unit-cell has been assumed to be embedded in a periodic lattice, and the magnitude and phase of the transmission coefficient have been computed with CST MW Studio as a function of W, for several frequencies in the band of interest (Ka-band). The simulated structure is shown in Fig. 2c. The unit-cell is surrounded by periodic boundaries that provide the infinite array conditions and take into account the mutual coupling between the cells. At this stage, a normal incidence plane wave has been considered. The selected dielectric material is RT-Duroid 6006 with a permittivity of $\varepsilon_r = 6.15$ and $\tan\delta = 0.0027$. Note that this choice has been taken to study the proposed unit-cell and to demonstrate its improved performances. Moreover, the high permittivity material allows to have a reduced total thickness. However, in view of the manufacturing of an antenna prototype, this type of dielectric is not the most suitable: possible solutions for the TA fabrication will be discussed in Sect. III.

The parametric analysis led to the definition of a unit-cell characterized by $L = \lambda_0/4 = 2.5$ mm, at $f_0 = 30$ GHz, $h_1 = 4.5$ mm and $h_2 = 4.5$ mm. The overall thickness of the element is therefore $T = h_1 + 2\,h_2 = 13.5\text{ mm} = 1.35\lambda_0$. The value chosen for h_2 guarantees a good matching and it provides a phase range of 360°.

The variations of the amplitude and the phase of S_{21} with W, for different frequencies, are presented in Figs. 3a and 3b, respectively. The plot in Fig. 3a proves that the matching layers guarantee a value of $|S_{21}|$ equal to -0.75 dB in the worst case. The phase range of the transmission coefficient obtained varying W in the interval $(0.1 \div 2.3)$ mm is greater than 360° at all the considered frequencies, as pointed out in Fig. 3b. The good bandwidth of the single cell can be also inferred from the frequency behavior of the transmission coefficient magnitude, shown in Fig. 4, where it is plotted for several values of W in the considered interval of variation. For all the considered values of W, $|S_{21}|$ is never lower than -1 dB in the analyzed frequency range. The best matching is achieved when W is maximized since the presence of dielectric in the cell is minimum and the value of the characteristic impedance becomes close to the free-space one.

B. TRANSMITARRAY DESIGN AND ANALYSIS

To test the actual effectiveness of the proposed unit-cell, three transmitarrays with different size have been designed at $f_0 = 30$ GHz and numerically analyzed. Each TA unit-cell is designed to compensate the spatial phase delay from the feed horn to the element itself [1], i.e. to provide a phase φ_i given by:

$$\varphi_i = k_0(R_i - \underline{r}_i \cdot \hat{r_o}) + \varphi_o \qquad (1)$$

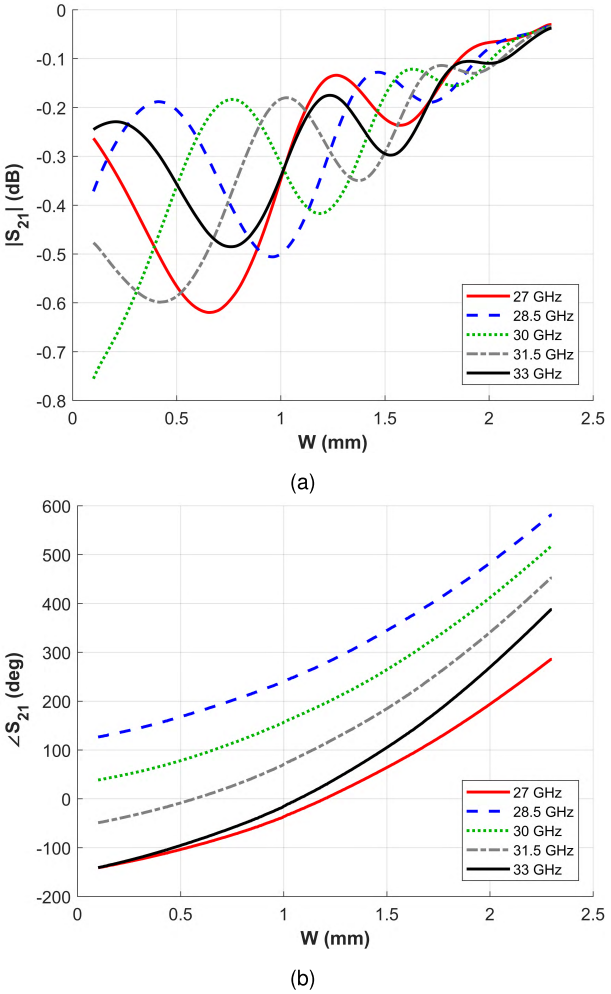

FIGURE 3. Simulated transmission coefficient as a function of W for different frequencies: (a) Amplitude $|S_{21}|$; (b) Phase $\angle S_{21}$.

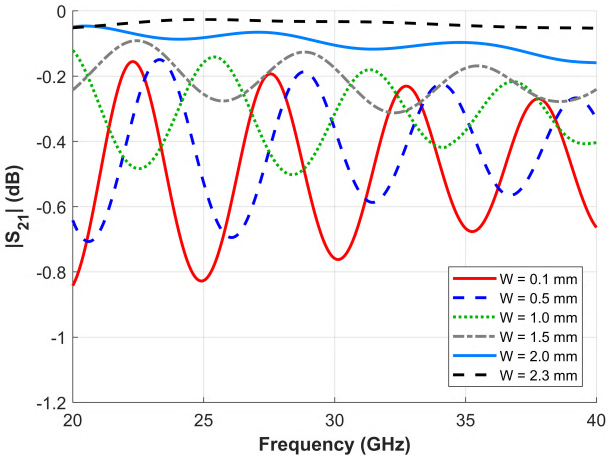

FIGURE 4. Simulated frequency behavior of the transmission coefficient amplitude for different W.

where k_0 is the propagation constant in free-space, R_i is the distance from the feed to the i-th element, whose position is located by $\underline{r}_i$, and $\hat{r_o}$ is the unit vector pointing to the

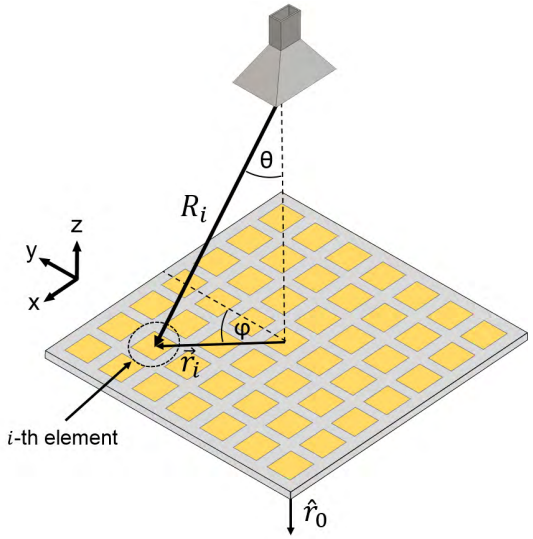

FIGURE 5. Typical geometry of a transmitarray antenna.

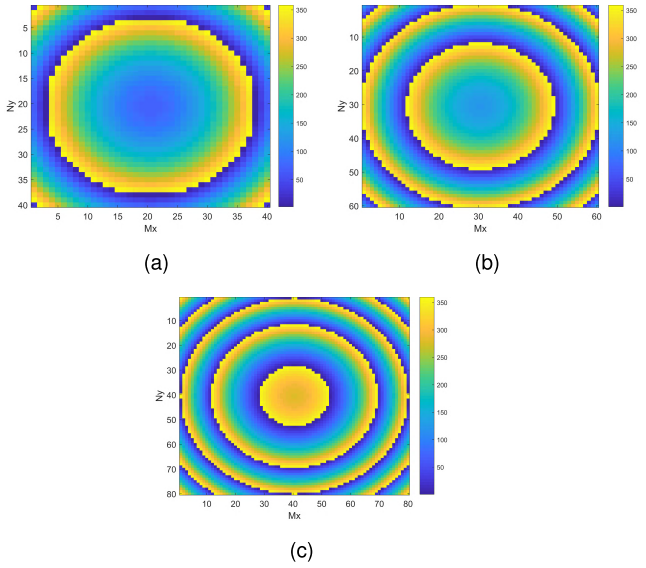

FIGURE 6. Required phase distribution for the three designed TA configurations: (a) 40×40 elements TA; (b) 60×60 elements TA; (c) 80×80 elements TA.

direction of maximum radiation. In the case considered here, the main beam direction is assumed to be the broadside one, therefore $\underline{r}_i \cdot \hat{r_o} = 0$ (see Fig. 5). The quantity φ_o is a constant phase value, indicating that a relative phase rather than the absolute one can be used for the transmitarray design. In each considered configuration, the transmitarray is a center-fed square structure with side D and $F/D = 0.9$, being F the distance between the feed and the TA (see Fig. 7a). The feed is a rectangular horn designed to have a 1-dB gain bandwidth in the frequency interval (27÷33) GHz, and the HPBW (Half-Power Band Width) almost equal in the E and H plane ($\theta_E = 32.3°$, $\theta_H = 32.4°$). Moreover, the horn has a gain of 14.4 dB at 30 GHz, it radiates a vertically polarized field, and its pattern can be approximately modelled as $cos^q(\theta)$, with $q = 7.7$. The chosen horn and its distance from the TA guarantees a taper of −11.7 dB.

The first designed TA, indicated as TA1 in the following, has a size of $D = 10\lambda_0 = 100$ mm and it is composed by 40×40 = 1600 elements. The second configuration (TA2) is characterized by a size $D = 15\lambda_0 = 150$ mm, corresponding to a structure of 60×60 = 3600 cells. Finally, the third one (TA3) is an array of 80×80 = 6400 elements with a total size of $D = 20\lambda_0 = 200$ mm. The resulting required phase-shift distribution of the three arrays, obtained using the equation (1), are represented in Figs. 6a, 6b, 6c. Notice that they do not differ only for the number of phase jump required by the increasing size, but also because of a different value of φ_o used.

The three structures have been simulated using CST MW Studio. The CST model of the medium size antenna (TA2) is sketched in Fig. 7. The front view in Fig. 7b highlights how the size variation of the central layer holes follows the required phase distribution plotted in Fig. 6b, with the smallest holes represented by the darker regions in the picture.

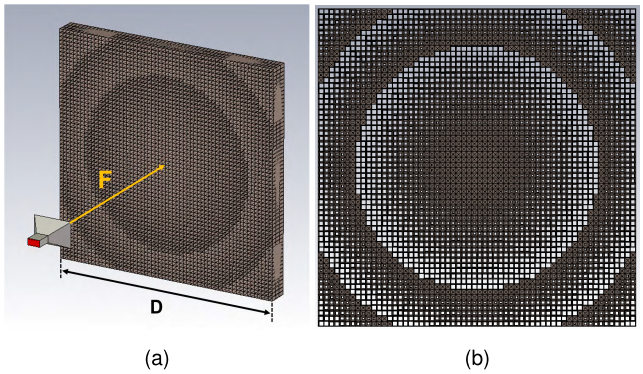

FIGURE 7. Sketch of the designed TA with size $D = 150$ mm $= 15\lambda_0$: (a) Perspective view of the CST antenna model; (b) Front view of the TA only.

In Fig. 8, the result of a first check on the proper functioning of the designed TAs is shown. In fact, it demonstrates the correct design of the medium size TA through its actual capability to transform the spherical wave radiated by the feed and impinging on the TA itself, in a plane wave.

The co- and cross-polarized radiation patterns in both the E- and H-plane computed at 30 GHz are plotted in Figs. 9, 10 and 11, for the solutions TA1, TA2 and TA3 respectively, while their main features are summarized in Table 1. From Fig. 9 and the second column in Table 1, it emerges that the radiation patterns of the solution TA1 have an HPBW of 6.1° in H-plane (Fig. 9a) and 6° in E-plane (Fig. 9b). The Side Lobe Level (SLL) is −19.1 dB in H-plane and −18.3 in E-plane, while the cross-polarization levels in the two planes are −25.1 dB and −26.5 dB, respectively. The second TA is characterized by the same HPBW in both planes, equal to 4° (Figures 10a, 10b and third column

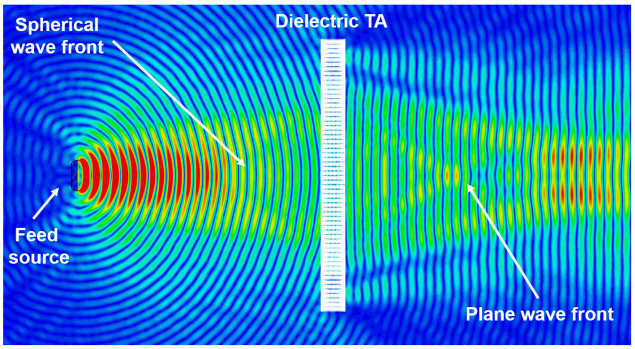

FIGURE 8. Field radiated by the transmitarray TA2.

TABLE 1. Summary of the radiation features of the three designed TAs.

Feature (at 30 GHz)	TA1	TA2	TA3
Gain	27.1 dB	31.1 dB	33.6 dB
1-dB Gain BW	30.9%	27.4%	17.5%
Ap. Efficiency	41.4%	45.3%	46%
HPBW (H-plane)	6.1°	4°	2.9°
HPBW (E-plane)	6°	4°	2.8°
SLL (H-plane)	-19.1 dB	-21.6 dB	-21 dB
SLL (E-plane)	-18.3 dB	-22 dB	-20.7 dB
X-pol level (H-plane)	-25.1 dB	-33.2 dB	-34.5 dB
X-pol level (E-plane)	-26.5 dB	-37.7 dB	-33.8 dB

in Table 1). Moreover, it exhibits very good performances in terms of side lobe and cross-polarization levels: SLLs are −21.6 dB (H-plane) and −22 dB (E-plane), while the cross-pol level is below −32 dB and −33 dB, respectively. Finally, the largest structure (TA3) provides radiation patterns with HPBW of 2.9° in H-plane and 2.8° in E-plane. The side lobe and cross-pol levels derived from Figures 11a and 11b and reported in the fourth column of Table 1, are equal to −21, −20.7, −34.5 and −33.8 dB, respectively. Due to its smaller size, the performances of the solution TA1 are slightly poorer than those of solutions TA2 and TA3, especially for what concerns the cross-polarization.

In Figs. 12a, 12b, the frequency behavior of the gain and of the aperture efficiency for the three configurations are shown. The results confirm the positive effect of the proposed unit-cell on the TA bandwidth. The 1-dB bandwidth achieves the 17.5% for the $20\lambda_0 \times 20\lambda_0$ antenna, the 27.4% for the $15\lambda_0 \times 15\lambda_0$ and the 30.9% for the $10\lambda_0 \times 10\lambda_0$, as listed in Table 1. For what concerns the (computed) efficiency, it is higher than 40% at the design frequency for all the three configurations (see Fig. 12b); at the extremes of the considered frequency interval, it is still higher than 30% for the configurations TA2 and TA3, while it is around 25% for the largest TA.

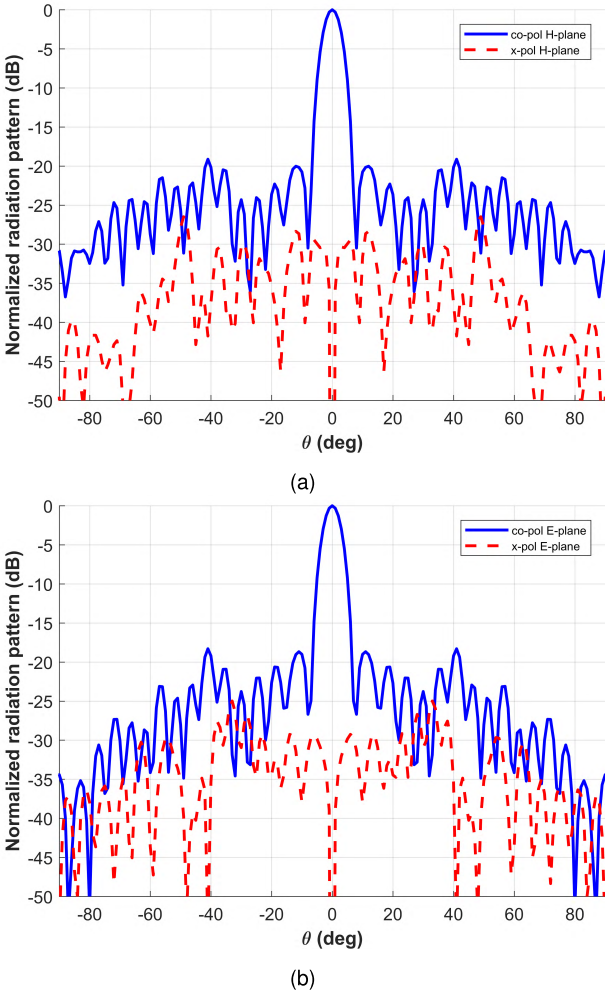

FIGURE 9. Simulated co- and cross-polar radiation patterns of the 40 × 40 TA (TA1), at 30 GHz: (a) H-plane; (b) E-plane.

III. PROTOTYPE MANUFACTURING AND EXEPERIMENTAL CHARACTERIZATION

In order to have a further validation of the proposed unit-cell, a prototype of the dielectric transmitarray has been manufactured and experimentally characterized. The best suited solution for the TA fabrication seems to be the use of an Additive Manufacturing (AM) technique, since the use of a conventional dielectric, as the one considered in the numerically analyzed configurations, would require to make the variable size holes and this is impracticable by conventional machining approaches, especially at millimeter-waves. However, the exploitation of 3D-printing techniques implies some limitations listed below.

- *Dielectric material*: the materials available for 3D-printing techniques are typically based on UV cross-linkable polymers, usually not optimized to provide functional (dielectric) properties. This means that such materials usually exhibit a dielectric constant not higher than 4.5. The limited value of permittivity implies an increase of the total thickness, since the effective wavelength depends on the dielectric constant and the

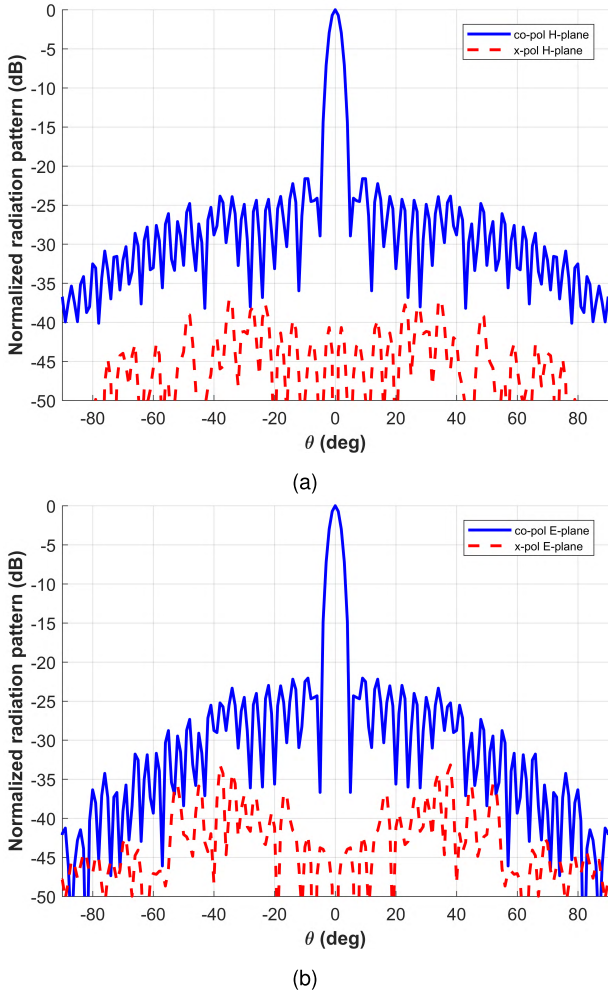

FIGURE 10. Simulated co- and cross-polar radiation patterns of the 60 × 60 TA (TA2), at 30 GHz: (a) H-plane; (b) E-plane.

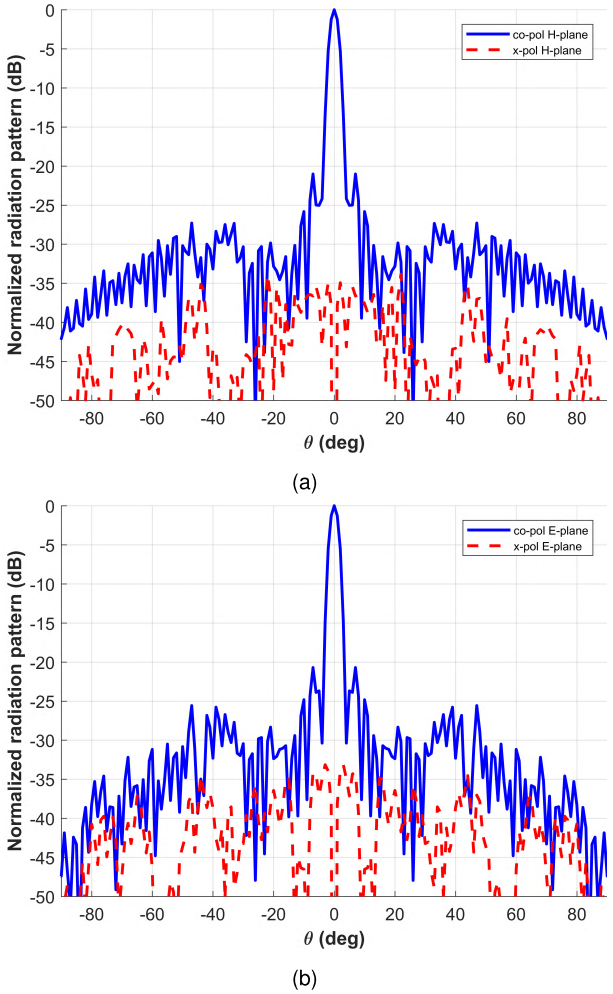

FIGURE 11. Simulated co- and cross-polar radiation patterns of the 80 × 80 TA (TA3), at 30 GHz: (a) H-plane; (b) E-plane.

filling factor. In most cases, they have also high losses over 10 GHz that affect the efficiency of the transmitarray and could reduce the bandwidth.

- *Geometry constraints*: the limited resolution of the current 3D-printers (>10 μm) does not allow to fabricate small features as those required at high frequencies, such as millimeter-waves. Due to its complexity, it is necessary to slightly change the geometry of the proposed TA element in order to make it 3D-printable.

In the next subsections, these aspects are taken into account with the goal of realizing a 3D-printed transmitarray prototype.

A. ADDITIVE MANUFACTURING

Additive Manufacturing is a relatively new class of processing technologies targeting breakthrough advancements for rapid prototyping and low to medium volume fabrication. It is also often regarded as a unique technological option for the fabrication of complex 3D objects skipping complex and time-consuming assembly procedures.

The Addititve Manufacturing technique employed for the fabrication of the TA belongs to the family of the 3D Printing Technology [18]–[22].

The proposed antenna was fabricated using the commercial printer Objet30 by Stratasys® along with the commercial resin VeroWhitePlus (RGD835 from Stratasys®). The printer is based on the so-called PolyJet technology: a printing head travels along the XY plane depositing thin layers of liquid resin, which are immediately polymerized by a UV lamp installed on board. The 3D printed object grows layer-by-layer: thanks to the vertical movement of the printing platform, that moves downward, each time a new resin layer is jetted. The nominal build accuracy is 600 dpi × 600 dpi on XY plane with a minimum layer thickness of 28 μm. This kind of printer uses also a second resin that acts as a support material (Support SUP705 from Stratasys®) and that is completely removed, at the end of the process, by water jet. Two options are available in the 3D printer pre-processing proprietary software: to completely wrap the whole object with the Support (“*matte*” option), or to use it only where

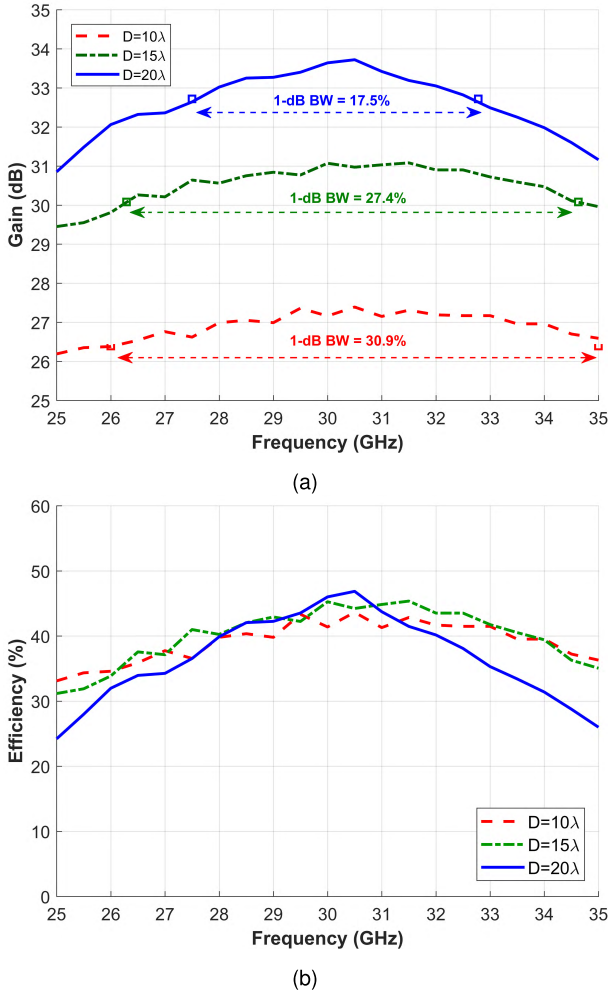

FIGURE 12. Frequency behavior of the gain (a) and the aperture efficiency (b) for the three considered TAs.

necessary to hold overhangs (''*glossy*'' option). Preliminary printing tests demonstrated that the *glossy* option better fits our case than the *matte* option. Indeed, since the proposed solution has tiny holes and tight cavities, the latter would produce parts too difficult to clean for proper Support removal, thus affecting the final geometry.

B. MODIFIED UNIT-CELL

In view of the requirements previously discussed, the unit-cell presented and analyzed in Section II has to be slightly modified. The first consideration concerns the limited resolution of the nozzle printer, that makes impossible to generate sharp edges as those located at the junction between two consecutive cells (see Fig 13). Moreover, the holes cannot be too small, otherwise during the printing process some polymeric residues may deposit into, plugging them and modifying the structure. To minimize this drawback, the minimum size of the holes must be increased (see Fig. 13).

These considerations lead to the introduction of a new unit-cell, named *type 2* in the following, to distinguish it from

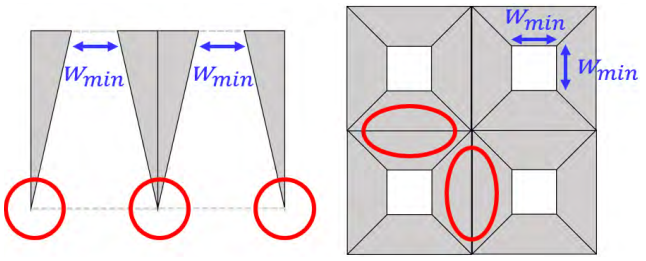

FIGURE 13. Geometry aspects of the unit-cell that have to be modified to obtain a 3D-printable structure.

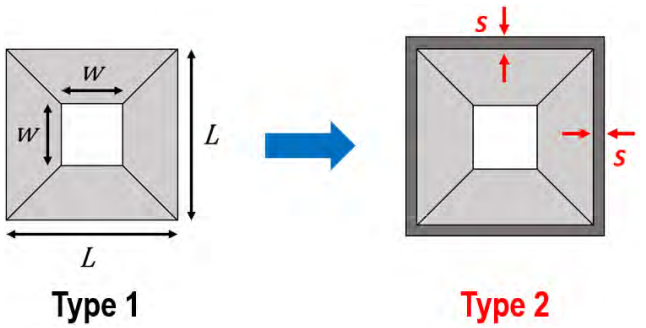

FIGURE 14. Comparison between the initial unit-cell (type 1) and the modified dielectric element (type 2) including additional lateral walls with a thickness S.

TABLE 2. Comparison of the geometric parameters for the different dielectric unit-cells expressed in mm.

Parameter (mm)	RT Duroid 6006 (type 1)	VeroWhitePlus (type 1)	VeroWhitePlus (type 2)
L	2.5	3	3
S	/	/	0.175
W	0.1 - 2.3	0.1 - 2.8	0.5 - 2.65
h_1	4.5	9.5	11
h_2	4.5	9.5	11
T	13.5	28.5	33

the original one (*type 1*): both of them are shown in Fig. 14. Comparing the two unit-cells, it appears that *type 2* has been derived from *type 1* adding a thicker wall between two consecutive cells. Its insertion allows to flatten the edges and to achieve a more physically printable structure. However, it affects the matching and the bandwidth performances, since the impedance at the interfaces between the unit-cell and the free-space is now slightly lower than 120π. After several printing tests and checking simulations, a good trade-off between printable constraints and valuable performances has been found. The selected value for the thin walls between consecutive cells is $S' = 2S = 300\ \mu m$. For what concerns the width of the holes, it has been fixed to $W_{min} = 500\ \mu m$, which is 5 times greater than the minimum size of the holes in the *type 1* unit-cell ($100\ \mu m$).

In view of these modifications, it was necessary to perform again the numerical characterization of the unit-cell. To better understand what are the effects of the change of the material and the geometrical variation, two different unit-cells have been analyzed: a *type 1* element in VeroWhitePlus material and a *type 2* unit-cell also made-up by VeroWhitePlus dielectric. Before the numerical analysis of the new unit-cell, the electromagnetic characterization of the dielectric material VeroWhitePlus has been performed using the waveguide method. The dielectric properties have been obtained from the transmission response of a 3.4 mm slab in the WR34 waveguide. The medium value found for the dielectric constant is $\varepsilon_r = 2.77$, while the loss tangent is $\tan\delta = 0.021$.

To achieve results similar to those reported in Figs 3 and 4, for both the phase variation and the matching in the same frequency range, the total thickness T of the unit-cell has been considerably increased due to the dielectric constant material decreased from 6.15 to 2.77 and for the geometrical constraints that *type 2* element has to satisfy. The height of the tapered section (h_2) and central layer (h_1) have been heightened to 9.5 mm for *type 1* in VeroWhitePlus and 11 mm for the *type 2*, respectively. The section L of the single cell has been changed from 2.5 mm to 3 mm, for both the cells made by VeroWhitePlus. A comparison of the geometrical parameters for the three considered cases is summarized in Table 2.

The new unit-cells have been simulated with CST MW Studio using the same method explained in Section II-A. The Fig. 15a shows a comparison of the transmission coefficient amplitude of the three cases, computed at 30 GHz. As expected, the use of VeroWhitePlus material consistently reduces the amplitude of S_{21}, since it has higher losses than Duroid 6006 and moreover the lower ϵ_r required an increase of the unit-cell thickness, as already pointed out. Therefore, $|S_{21}|$ is reduced of almost 2 dB for the type 1 unit-cell and of almost 2.5 dB for the type 2. In Fig 15b, the transmission coefficient phases for the three unit-cells are compared. Despite the constraints imposed by the printing technology, the slope of the curves remains quite the same also for the VeroWhitePlus-based elements, because the thickness has been increased to guarantee a full phase variation of 360°.

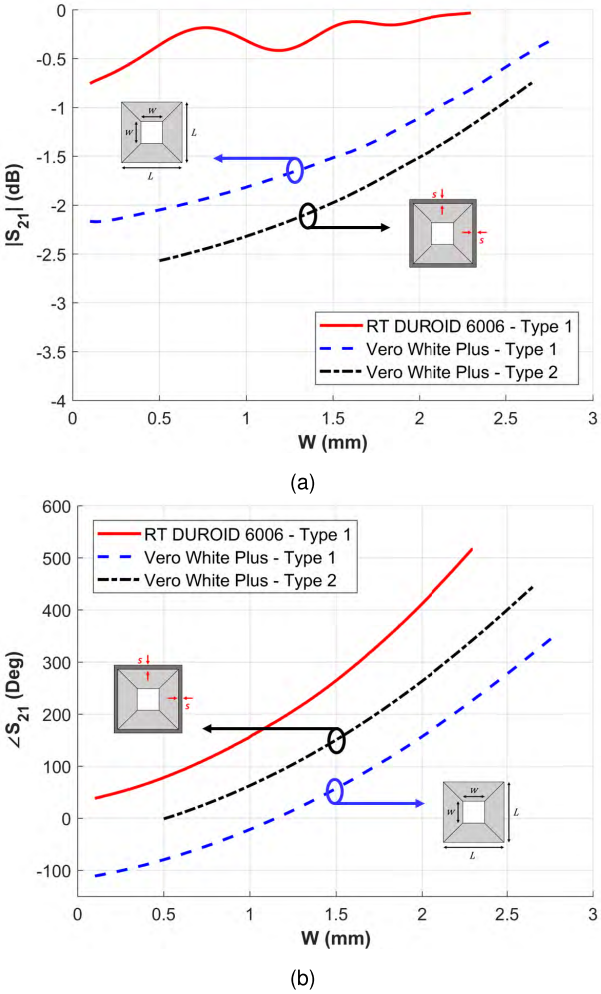

FIGURE 15. Comparison of the simulated transmission coefficients for different unit-cells as a function of W computed at 30 GHz: (a) Amplitude $|S_{21}|$; (b) Phase $\angle S_{21}$.

C. 3D-PRINTED WIDEBAND TRANSMITARRAY

The type 2 unit-cell presented in the previous section has been used to design and manufacture a 3D-printable Transmitarray. This prototype, indicated in the following as configuration TA4, is still a center-fed and centered beam square structure. Its size is $D = 15.6\lambda_0 = 156$ mm, corresponding to $52\times52 = 2704$ elements, and it matches with the maximum area printable in a single piece. The used feed is a circular horn designed to work in Ka-band and it is positioned at 156 mm from the TA ($F/D = 1$). The horn has a gain of 17 dB at 30 GHz, the HPBW in E and H plane equal to $\theta_E = 25.4°$, $\theta_H = 25.1°$, while its pattern can be modelled as $cos^q(\theta)$, with $q = 12.5$.

Since the antenna is symmetric along a horizontal plane cutting the structure at half of the thickness, a specific printing strategy was adopted to simplify and optimize the printing process. This is because the upper half has pyramidal cells oriented downwards, while the lower half has pyramidal cells oriented upwards, so during printing the lower half would have overhangs which would be necessarily supported by Support resin, even in case of glossy option selection. For this reason, the 3D layout of the proposed antenna was cut into two halves, which were printed separately with the pyramidal cells always oriented downwards. Due to the tray size limit of the Object 30, each half takes 6 hours to be printed. Therefore, a complete 3D printed antenna was obtained after 12 hours. Twelve lateral junction rings were added to the original design, three per side for each half, as reported in Fig. 16. In such way, the two halves could be easily assembled at the end of the printing process by twelve nylon M3 screws. The alignment between the two parts was ensured by the printer build accuracy. Four of the external rings were also employed to fix the TA to the feed structure. The final 3D-printed TA prototype is presented in Fig. 16, while a

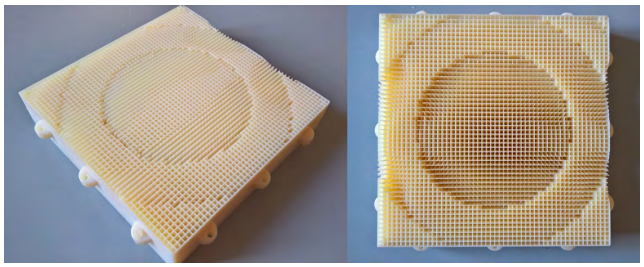

FIGURE 16. Pictures of the 3D-printed prototype.

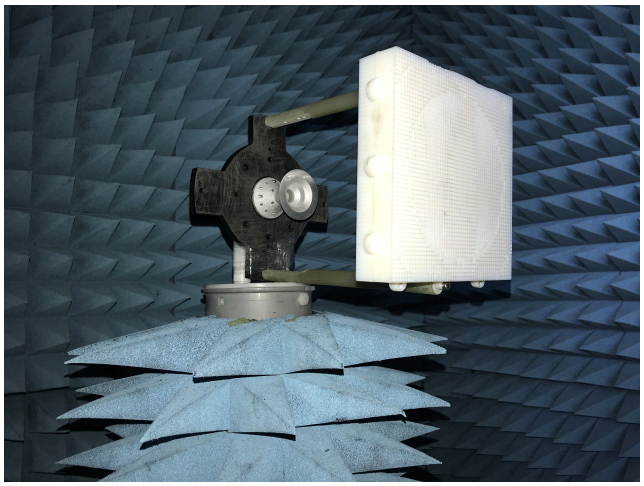

FIGURE 17. Measurement setup in the anechoic chamber.

picture of the entire antenna is shown Fig 17. It has been simulated with CST MW Studio, without the supporting structure, and then experimentally characterized.

The simulated and measured radiation patterns in E- and H-plane are shown in Figs 18a and 18b, respectively. From these graphs, it can be observed a good a good agreement between simulations and measurements. Both the radiation patterns exhibit a 3dB-beamwidth of 4° in the two principal planes, while the SLL is even better for the measured patterns, being equal to −22.6 dB in the E-plane and −21.6 dB in the H-plane.

In Fig. 19 the frequency behavior of the measured gain and aperture efficiency are shown: as it appears, the prototype confirmed the good results already obtained by the numerical analysis of configurations TA1-TA3, since it is characterized by a 1-dB bandwidth still larger than 20%. Moreover, it is almost coincident with the computed one (21.5% against 21.7%). The reduced values of gain and efficiency with respect to the antenna TA2, that has a comparable size, must be ascribed to the higher losses of the VeroWhitePlus material and to the need to use a thicker TA.

Finally, in Table 3, the main features of the four configurations are summarized and compared with results available in literature for other TAs by analogous size D and ratio F/D. Configuration TA1, the smallest of the designed antennas, has a size comparable with the TA in [10], even if this latter

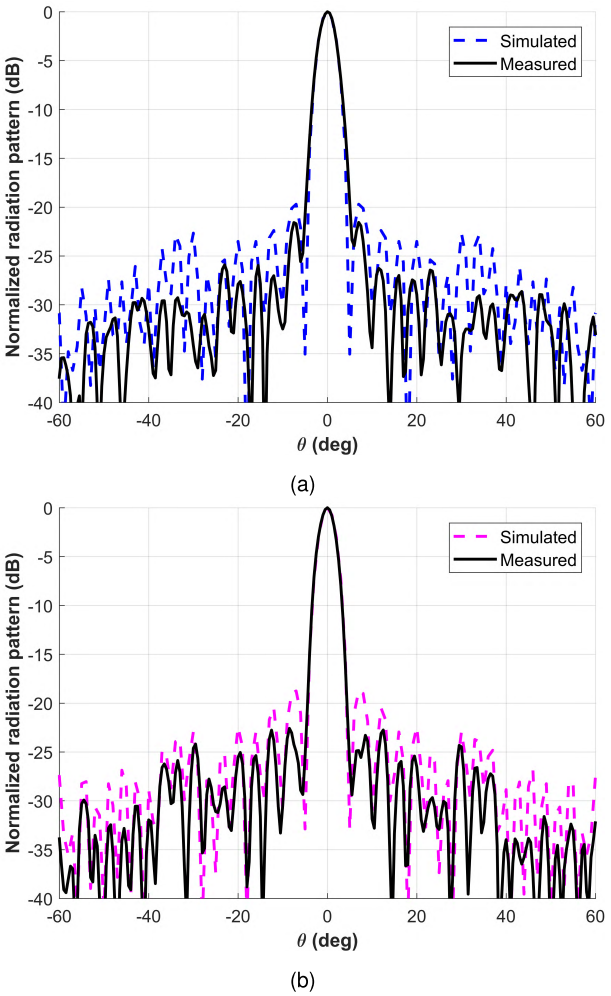

FIGURE 18. Measured and simulated co-polar radiation patterns of the 3D-printed TA prototype (TA4), at 30 GHz: (a) H-plane; (b) E-plane.

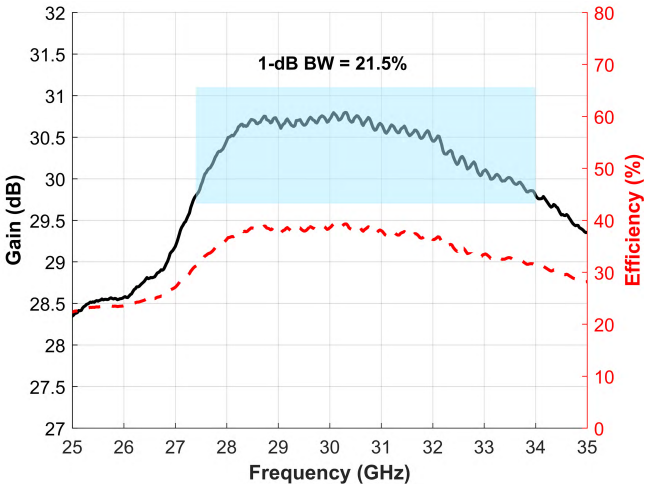

FIGURE 19. Measured frequency behavior of the gain and aperture efficiency for the 3D-printed TA prototype (TA4).

is circular: therefore, its area is significantly lower and this impacts on the aperture efficiency. Indeed, while TA1 has not only a 1-dB bandwidth that is almost double, but also a

TABLE 3. Main features of the designed transmitarrays and comparisons with results available in literature for other proposed solutions.

Ref.	Freq (GHz)	F/D	Overall Thickness (λ_0)	TA area (λ_0^2)	Gain (dB)	Aperture eff. (%)	1-dB Gain BW (%)
[4]	30.25	0.9	0.96	12.6×12.6	28.6	47%	7.5%
[5]	11.3	0.8	0.51	$(8.1)^2\pi$	28.9	30%	9%
[6]	12.5	0.76	0.52	5.4×5.4	18.9	20.9%	9.6%
[7]	13.5	0.95	0.76	$(7.24)^2\pi$	29.9	47%	11.7%
[8]	10.3	0.8	0.43	6.4×6.4	24.8	55%	15.5%
[9]	61.5	0.7	1.7	$(10.25)^2\pi$	32.5	42.7%	15.4%
[10]	12.4	1	0.62	$(4.6)^2\pi$	25.8	46.5%	16.8%
[14]	94	0.77	1.31	18.2×18.2	30	25%	15.9%
[15]	60	0.42	2	9.5×9.5	23.5	20%	17%
TA1	30	0.9	1.35	10×10	27.1	41.4%	30.9%
TA2	30	0.9	1.35	15×15	31.1	45.3%	27.4%
TA3	30	0.9	1.35	20×20	33.6	46%	17.5%
TA4	30	1	3.3	15.6×15.6	30.7	38.6%	21.5%

higher maximum gain, its aperture efficiency is 5% smaller. TA1 can be also compared with the configuration in [15], with respect to which it presents better performances. Solutions TA2 and TA4 have a size similar to the structures in [4] and in [7], whose performances are summarized in rows 1 and 4 of the table. Both of them have a 1-dB bandwidth much narrower than the one of the solution TA2, which is 27.4% (see row 11 of Tab. 3 and Fig. 12a) and of the prototype TA4 (row 13 in Table 3), that is equal to 21.5%. However, both the solution presented here, and in particular the prototype TA4, have a lower efficiency. As already mentioned, in the case of the manufactured configuration, this is due to the higher losses in the material and the increased thickness.

Comparing those of the considered configurations, reported in the third column of the table, it emerges that the limitations of the AM techniques, especially at high frequencies, are still related to the reduced set of available dielectric material and to the printer resolution. In fact, the two thicker configurations among those considered are TA4 and the TA in [15], both manufactured with a 3D-printer. This points out the need to develop 3D-printable dielectric materials with better properties. For what concerns the largest TA (TA3), it can be compared with the antennas in [9] and [14]: the solution proposed here outperforms the other two for what concerns the bandwidth, the gain and the efficiency.

IV. CONCLUSION AND DISCUSSION

In this paper, a novel three-layer unit-cell for Transmitarray Antennas has been introduced and analyzed. Its main feature is an enhanced bandwidth, obtained by exploiting the tapered matching concept. This new element has been used to design three different sized TA configurations. They have been numerically characterized and the obtained results confirm that their performances in terms of bandwidth outperform those of other antennas available in literature. To further validate the unit-cell features, the possibility of its manufacturing with a 3D-printing technique has been exploited. It emerged that to make it possible, significant modifications of the unit-cell was necessary in order to take into account both the dielectric characteristics of the 3D-printable material and the current resolution of the state-of-the-art 3D printers. A medium-size prototype working on a band centered at 30 GHz has been finally manufactured and experimentally characterized: the obtained results confirm the good performances of the proposed configuration, achieving a 1-dB bandwidth of 21.5% and an aperture efficiency of 38.6%. The antenna features could be further enhanced when dielectric material with higher value of ϵ_r will be available for high resolution printers.

REFERENCES

[1] A. H. Abdelrahman, F. Yang, A. Z. Elsherbeni, and P. Nayeri, *Analysis and Design of Transmitarray Antennas*. M&C Publishers, 2017.
[2] D. M. Pozar, "Flat lens antenna concept using aperture coupled microstrip patches," *Electron. Lett.*, vol. 32, no. 23, pp. 2109–2111, Nov. 1996.
[3] W. An, S. Xu, F. Yang, and M. Li, "A double-layer transmitarray antenna using malta crosses with vias," *IEEE Trans. Antennas Propag.*, vol. 64, no. 3, pp. 1120–1125, Mar. 2016.
[4] C. G. M. Ryan, M. R. Chaharmir, J. Shaker, J. R. Bray, Y. M. M. Antar, and A. Ittipiboon, "A wideband transmitarray using dual-resonant double square rings," *IEEE Trans. Antennas Propag.*, vol. 58, no. 5, pp. 1486–1493, May 2010.
[5] A. H. Abdelrahman, A. Z. Elsherbeni, and F. Yang, "High-gain and broadband transmitarray antenna using triple-layer spiral dipole elements," *IEEE Antennas Wireless Propag. Lett.*, vol. 13, pp. 1288–1291, Jul. 2014.
[6] J. Yu, L. Chen, J. Yang, and X. Shi, "Design of a transmitarray using split diagonal cross elements with limited phase range," *IEEE Antennas Wireless Propag. Lett.*, vol. 15, pp. 1514–1517, Jan. 2016.

[7] A. H. Abdelrahman, P. Nayeri, A. Z. Elsherbeni, and F. Yang, "Bandwidth improvement methods of transmitarray antennas," *IEEE Trans. Antennas Propag.*, vol. 63, no. 7, pp. 2946–2954, Jul. 2015.

[8] B. Rahmati and H. R. Hassani, "High-efficient wideband slot transmitarray antenna," *IEEE Trans. Antennas Propag.*, vol. 63, no. 11, pp. 5149–5155, Nov. 2015.

[9] C. Jouanlanne *et al.*, "Wideband linearly polarized transmitarray antenna for 60 GHz backhauling," *IEEE Trans. Antennas Propag.*, vol. 65, no. 3, pp. 1440–1445, Mar. 2017.

[10] C. Tian, Y.-C. Jiao, G. Zhao, and H. Wang, "A wideband transmitarray using triple-layer elements combined with cross slots and double square rings," *IEEE Antennas Wireless Propag. Lett.*, vol. 16, pp. 1561–1564, Jan. 2017.

[11] A. Petosa and A. Ittipiboon, "Design and performance of a perforated dielectric Fresnel lens," *IEE Proc.-Microw., Antennas Propag.*, vol. 150, no. 5, pp. 309–314, Oct. 2003.

[12] S. H. Zainud-Deen, S. M. Gaber, and K. H. Awadalla, "Transmitarray using perforated dielectric material for wideband applications," *Prog. Electromagn. Res. M*, vol. 24, pp. 1–13, 2012.

[13] M. K. T. Al-Nuaimi and W. Hong, "Discrete dielectric reflectarray and lens for E-band with different feed," *IEEE Antennas Wireless Propag. Lett.*, vol. 13, pp. 947–950, 2014.

[14] A.-E. Mahmoud, W. Hong, Y. Zhang, and A. Kishk, "W-band mutlilayer perforated dielectric substrate lens," *IEEE Antennas Wireless Propag. Lett.*, vol. 13, pp. 734–737, 2014.

[15] H. Yi, S.-W. Qu, K.-B. Ng, C. H. Chan, and X. Bai, "3-D printed millimeter-wave and terahertz lenses with fixed and frequency scanned beam," *IEEE Trans. Antennas Propag.*, vol. 64, no. 2, pp. 442–449, Feb. 2016.

[16] M. Wang, S. Xu, F. Yang, and M. Li, "Design of a Ku-band triple-layer perforated dielectric transmitarray antenna," in *Proc. IEEE Int. Symp. Antennas Propag.*, Fajardo, Puerto Rico, Jun./Jul. 2016, pp. 1381–1382.

[17] R. E. Collin, *Foundations for Microwave Engineering*, 2nd ed. New York, NY, USA: McGraw-Hill, 1992.

[18] T. D. Ngo, A. Kashani, G. Imbalzano, K. T. Q. Nguyen, and D. Hui, "Additive manufacturing (3D printing): A review of materials, methods, applications and challenges," *Compos. B, Eng.*, vol. 143, pp. 172–196, Jun. 2018.

[19] V. Bertana *et al.*, "3D-printed microfluidics on thin poly(methyl methacrylate) substrates for genetic applications," *J Vac. Sci. Technol. B*, vol. 36, no. 1, 2018, Art. no. 01A106.

[20] G. Gonzalez *et al.*, "Development of 3D printable formulations containing CNT with enhanced electrical properties," *Polymer*, vol. 109, pp. 246–253, Jan. 2017.

[21] M. D. Vecchio *et al.*, "Behaviour of the intraocular pressure during manual and vented gas forced infusion in a simulated pars plana vitrectomy," *Int. J. Appl. Eng. Res.*, vol. 12, no. 17, pp. 6751–6757, 2017.

[22] S. L. Marasso *et al.*, "PLA conductive filament for 3D printed smart sensing applications," *Rapid Prototyping J.*, vol. 24, no. 4, pp. 739–743, 2018, doi: 10.1108/RPJ-09-2016-0150.

ANDREA MASSACCESI (S'15) received the B.S. degree in electronic engineering from the Università Politecnica delle Marche, Ancona, Italy, in 2012, and the M.S. degree in electronic engineering from the Politecnico di Torino, Turin, Italy, in 2015, where he is currently pursuing the Ph.D. degree in electrical, electronic and communication engineering. His research activities include the study of underwater electromagnetic propagation and the design of proper antennas for underwater environments, the design of innovative transmitarray antennas, and the development of efficient global optimization techniques suitable for electromagnetic problems.

PAOLA PIRINOLI (M'96) received the M.S. (Laurea) and Ph.D. (Dottorato di Ricerca) degrees in electronic engineering from the Politecnico di Torino, Italy, in 1989 and 1993, respectively. In 1994, she joined the Politecnico di Torino as an Assistant Professor (Ricercatore) with the Department of Electronics and Telecommunications and has also been an Associate Professor since 2003. From 1996 to 1997, she was a Visiting Research Fellow with the University of Nice Sophia Antipolis, France. In 2014, 2015, and 2017, she was a Visiting Research Fellow with Tsinghua University, Beijing, China.

She has co-authored around 250 journal articles and conference papers. Her main research activities include the development of analytically based numerical techniques, essentially devoted to the fast and accurate analysis of printed structures on planar or curved substrates, the modeling of non-conventional substrates, as chiral and anisotropic ones, the development of innovative and efficient global optimization techniques, and the design of innovative reflectarrays and transmitarray antennas. She is a member of the TPC and the Organizing Committee of several Conferences. She serves as a reviewer for several International Journals and Conferences.

Dr. Pirinoli received the Young Scientist Award and the Barzilai Prize for the Best Paper at the National Italian Congress of Electromagnetic (XII RiNEm) in 1998 and the Prize for the Best Oral Paper on antennas at the Millennium Conference on Antennas and Propagation in 2000.

VALENTINA BERTANA received the B.Sc. and M.Sc. degrees in biomedical engineering from the Politecnico di Torino in 2013 and 2015, respectively, where she is currently pursuing the Ph.D. degree in electrical, electronic and communication engineering. Her research activities are mainly focused on additive manufacturing, smart materials, and printable electronics.

GIORGIO SCORDO received the B.Sc. degree in biomedical engineering from the Università Federico II di Napoli in 2012 and the M.Sc. degree in biomedical engineering from the Campus Biomedico di Roma in 2014. He is currently pursuing the Ph.D. degree in electrical, electronic and communication engineering with the Politecnico di Torino. His research activities are mainly focused on microfluidics, additive manufacturing, and smart materials.

SIMONE LUIGI MARASSO received the master's degree in biomedical engineering and the Ph.D. degree in electronic devices from the Politecnico di Torino, Turin, Italy, in 2005 and 2010, respectively. From 2005 to 2011, he had a fellowship with the Politecnico di Torino and he worked at the Chilab-Materials and Microsystems Laboratory, Chivasso, Italy. Since 2014, he has been a CNR Researcher with the DISAT Department, IMEM, Politecnico di Torino. His research activities focus on the design and fabrication of MEMS, Lab-on-Chip, and microfluidic devices as demonstrated by his scientific publications in these fields.

MATTEO COCUZZA graduated in electronic engineering from the Politecnico di Torino, Turin, Italy, in 1997, and the Ph.D. degree in electronic devices in 2003. Since 2004, he has been a Researcher of the IMEM-CNR. In 1998, he was one of the founders of the Chilab-Materials and Microsystems Laboratory, Politecnico di Torino. He is currently a Lecturer of master's degree courses related to MEMS, micro- and nano-technologies, also in the framework of the International Master Degree in Nanotechnologies for IC (joined master between the Politecnico di Torino, INPG Grenoble, and EPFL Lausanne). His research activity is focused on MEMS and microsensors for industrial applications, on the development of microfluidics and lab-on-a-chip for biomedical applications and, more recently, on the development and application of polymeric 3-D printing technologies.

GIANLUCA DASSANO received the Laurea degree in electronic engineering from the Politecnico di Torino, Italy, in 1999. Since 1999, he has been with the Department of Electronics and Telecommunications, Politecnico di Torino, as a Technician with the Electromagnetic Group, with particular interest in antenna application. At present, his main activities concern antenna prototyping and characterization inside the Laboratory of Antennas and EMC.